ADVANCED MATERIALS INTERFACES
www.advmatinterfaces.de

Strongly Coupled Interfaces between a Heterogeneous Carbon Host and a Sulfur-Containing Guest for Highly Stable Lithium-Sulfur Batteries: Mechanistic Insight into Capacity Degradation

Hong-Jie Peng, Ting-Zheng Hou, Qiang Zhang, Jia-Qi Huang, Xin-Bing Cheng, Meng-Qing Guo, Zhe Yuan, Lian-Yuan He, and Fei Wei*

The use of conductive frameworks as the host scaffold to obtain nanostructured sulfur cathodes is an efficient way to increase the sulfur utilization for redox reaction in Li-S batteries with large discharge capacity and high energy density. However, due to dynamical interfaces driven by phase evolution between the conductive hosts and S-containing guests during cycling, the cathode still faces poor stability. Herein, the use of O-/N-containing nanocarbon as the conductive host sheds a light on the role of the dynamic interface between the carbon host and S-containing guest for a stable Li-S cell. The outstanding reversibility and stability of N-doped C/S cathodes are attributed to the favorable guest-host interaction at the electron-modified interface, manifesting as (i) a chemical gradient to adsorb polar polysulfides and (ii) ameliorative deposition and recharging of Li_2S on the region of electron-rich pyridinic N and a graphene domain surrounding quaternary N. Highly reversible, efficient and stable Li storage properties such as mitigated polarization and charge barrier, high capacity of 1370 and 964 mAh g^{-1} at 0.1 and 1.0 C, respectively, and 70% of capacity retention after 200 cycles are achieved. Mechanistic insight into the capacity fading inspires the rational design on electrodes for high-performance electrochemical systems.

1. Introduction

High energy density storage technology is strongly considered for the broad use of portable electronic devices, the development of electric vehicles, as well as controllable energy harvest from renewable energy sources. The lithium–sulfur (Li-S) battery is a promising candidate due to the fact that elemental S offers a high theoretical specific capacity (1675 mAh g^{-1}) and, therefore, Li-S batteries demonstrate high theoretical energy density (2600 Wh kg^{-1} based on the electrochemical reaction 16 Li + S_8 = 8 Li_2S), which is 3 to 5 times higher than that of state-of-art Li-ion batteries based on intercalation chemistry.[1–3] The use of S as the cathode has the advantages of natural abundance, low cost, environmental benignancy, and a wide operating-temperature range. However, there are many basic obstacles to fully demonstrate the potential of S-based cathodes for a Li-S cell. Both S and lithium sulfides (Li_2S) are intrinsically insulative, leading to low utilization of active materials in the cathode and poor electrochemical reversibility. Remarkable volume changes during the charge-discharge cycle may also lead to the fracture of the conductive scaffold and detachment of the active phase. Meanwhile, the shuttle effect described as intermediate high-order polysulfides diffusing to the anode side, where they react with metallic lithium to form low-order polysulfides, and diffusing back lowers the efficiency, leads to irreversible loss of polysulfides, and corrodes the anode.[3] Consequently, the discharge capacity always decays rapidly.

The use of a conductive framework as the host scaffold to obtain a nanostructured composite S cathode is an efficient and effective way to increase the utilization of S for redox reaction.[2–4] Porous carbon,[5,6] carbon nanotubes (CNTs),[7,8] graphene,[9–11] conductive polymer,[12,13] as well as their hybrid framework[14–16] have all been employed. They can serve as the host scaffold to accommodate the S/Li_2S and demonstrate significant improvement for the cathode capacity. However, the capacity decay induced by the shuttle effect and the deterioration of full transformation to Li_2S still remains a great challenge. On one hand, the physical confinement of polysulfides by micropores,[16] protective layers,[17] inorganic reservoirs,[18] and the nanocarbon interlayer structure,[19] successfully demonstrated their effectiveness for confining/adsorbing polysulfides, retarding their rapid diffusion, and suppressing the shuttle effect in a Li-S cell. On the other hand, the introduction of a solid electrolyte,[20] a solvent-in-salt system,[21] or a lithium salt additive, such as lithium nitrate ($LiNO_3$),[22] can tune the dissolvability/precipitation of the S-containing compound and

H.-J. Peng, T.-Z. Hou, Prof. Q. Zhang, Dr. J.-Q. Huang, X.-B. Cheng, M.-Q. Guo, Z. Yuan, L.-Y. He, Prof. F. Wei
Beijing Key Laboratory of Green Chemical Reaction Engineering and Technology
Department of Chemical Engineering
Tsinghua University
Beijing 100084, PR China
E-mail: zhang-qiang@mails.tsinghua.edu.cn

DOI: 10.1002/admi.201400227

modify the surface layer and morphology of the Li metal anode. However, when the ionic diffusion rate is hindered, the performance of Li-S cells deteriorates. The key to improve the cycling performance with high capacity of a Li-S cell lies in obtaining control over the interaction between the conductive host framework and S-containing guests (e.g., S, polysulfide, and Li_2S) to achieve a stable surface reaction and phase evolution.

Generally, the phase evolution of S at the interface between the conductive host and S-containing guest always offers a dynamic equilibrium during the charge–discharge cycle. The topological factors of the host were considered to restrain the active phase,[5,7,11,15,16] but the surface chemistry, especially the role of heteroatoms, still requires detailed investigation.[10,23] Amphiphilic polymer modification,[24,25] functional binders,[26] and ionic selective separators[27] were employed to regulate the surface chemistry, chemically adsorb polysulfides on the cathode side, and shield their diffusion on the separator side, respectively. However, the additional modifications bring in electrochemically inactive mass, and thus hinder the full demonstration of energy density. In situ doping on conductive carbon framework by employing various N-doped mesoporous carbon was proved to favor the electrochemical reactions.[28] Since other conductive agents or ionic liquids were also introduced into the system and the topological benefit of sophisticatedly designed mesopores was considered, the role of doped heteroatoms is unclear yet. Recently, Song et al. proposed the synergistic effects of neighboring N-/O-containing groups in N-doped mesoporous carbon on enhanced interaction with elemental S for superior Li-S battery performance.[23,29] However, S in cathode always suffers inevitable phase evolution into soluble polysulfides and recrystallized Li_2S solids, which are generally recognized as more pivotal issue of capacity degradation than pristine S. Thus, the mechanistic insights on the interaction of S-containing species/doping N and phase/interface evolution during the whole electrochemical process are still not well understood yet. If the topological factor isn't considered in material design, the effect of doping will be more distinct. In fact, the heteroatom incorporated into the carbon framework renders the tunable electronic properties and hence gives rise to heterogeneous interfaces anticipated to significantly improve catalytic activities[30] and electrochemical performances.[23,31–33] In case of Li-S battery, an ideal conductive host framework not only can well accommodate the non-polar S, but also intrinsically attracts the polar Li_2S and polysulfides to circumvent its irreversible loss.

In this contribution, we employ the idea of the use of O- and N-containing nanocarbon as the conductive host to shed a light on the role of the heterogeneous interface between the chemically modified carbon host and S-containing guest for a stable Li-S cell. To provide the proof-of-the-concept, pristine CNTs, oxidized CNTs (OCNTs), and N-doped CNTs (NCNTs), which are mass-produced without sophisticated fabrication procedure as typical N-doped mesoporous carbon material for good physical confinement, are used as carbon hosts to accommodate S guests. The electrochemical redox reaction and concomitant phase evolution are depended on the interface between the host/guest. Especially the interaction between N-containing functional groups is expected to host the sulfur containing guests. By engineering the strongly-coupled interface based on NCNTs, the favorable capacity of 1370 and 964 mAh g^{-1} at 0.1 and 1.0 C (1.0 C = 1675 mA g^{-1}), excellent cycling stability over 70% during 200 cycles, good rate capability, and high reversibility are achieved. First-principle calculation reveals the enhanced interaction between N-modified carbon surface and S species at each stage of the whole discharge-charge process.

2. Results and Discussion

Both the CNTs and NCNTs were mass produced via fluidized-bed chemical vapor deposition (CVD). **Figure 1**a shows the typical morphology of CNTs as seamless tubular by coaxially rolling multi-layered graphene. With hetero-N atoms introduced into graphitic domain, a stacked nanocup-like structure is available but preserves the integrity along the *c*-axis for rapid electron transportation (Figure 1b). The chemical oxidation of CNTs using nitric acid endows the OCNTs with increased defects and exfoliated graphene layer while still sustain a nanocable-like morphology (Figure 1c). By N_2 isothermal adsorption/desorption, similar adsorption behavior, Brunauer-Emmett-Teller (BET) specific surface area around 2.0×10^2 m^2 g^{-1}, and pore structure of CNTs, NCNTs, and OCNTs shown in Figure S1 indicate compatible but limited physical confinement when these nanocarbons were employed as carbonaceous substrates for S-containing guests. Therefore, CNT-based nanocarbon is expected to be more suitable platform to investigate the effect of functional groups on Li-S chemistry than porous carbon due to its open pore structure and resulting poor spatial confinement on S species.

The doping/functionalization on CNTs mainly tend to mediate the surface chemistry of NCNTs and OCNTs rather than their ability of physical confinement. X-ray photoelectron spectroscopy (XPS) was employed to investigate their surface properties. Nitrogen peak is only observed in spectrum of NCNTs, suggesting the incorporation of N into the π-delocalization of sp^2-carbon (Figure 1d and S2a). With assistance of ammonia during CVD, the content of N in NCNTs reached 1.76 at%. The high-resolution N1s spectrum of NCNTs exhibits different heterogeneity of N-doping forms, which is deconvoluted into three predominant characteristic peaks of pyridinic N, quaternary N (N atoms coordinated in the graphene lattice in substitution of C), and chemisorbed N (Figure 1e).[33] By conducting fine scanning of O1s region, distinctly different surface properties of OCNTs against CNTs and NCNTs are detected (Figure S2b), indicating the functionalization of large quantities of O-containing groups with similar species such as hydroxyls, carbonyls, and ether groups except the greatly increased carboxyls. The relative amounts of N-/O-functional groups are listed in Table S1 and 2 for details.

To prepare the functionalized carbon based composite cathode material for Li-S batteries, S was infiltrated into nanocarbon via typical melting-diffusion strategy at 155 °C for 4.0 h. As-fabricated composites denote as CNT-S, NCNT-S, and OCNT-S, respectively. The X-ray diffraction (XRD) pattern of well-crystalline orthorhombic S in NCNT-S suggests that the open-structured interspace of NCNTs can only afford limited spatial confinement to S (**Figure 2**a). However, both the content and thermal stability of S in the composite are promoted remarkably after surface functionalization of carbon as

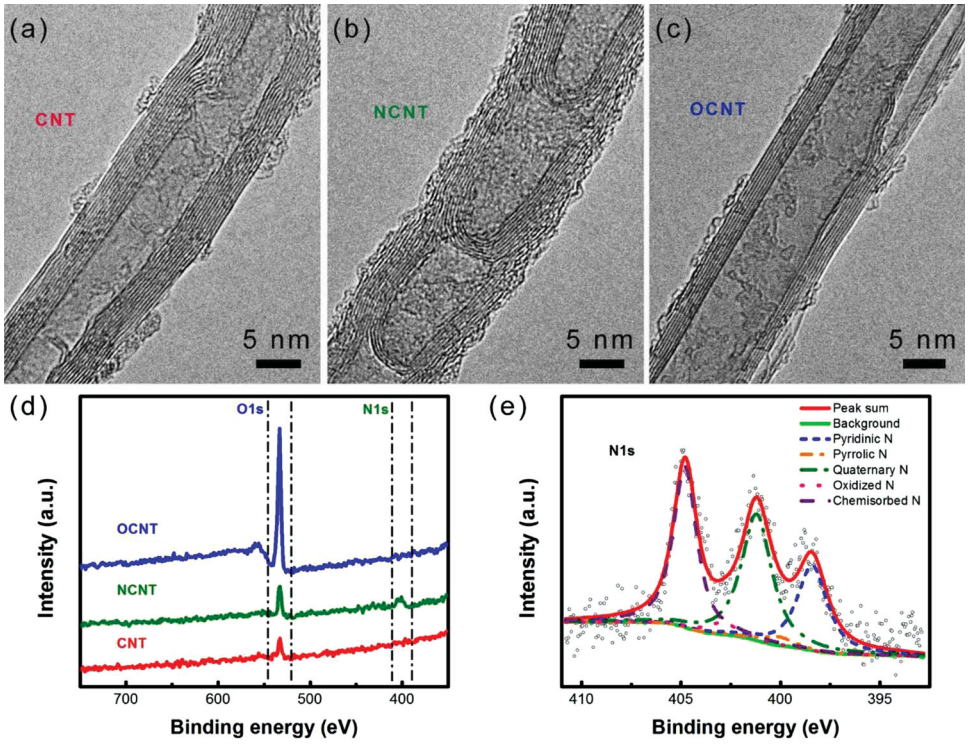

Figure 1. Morphology and heterogeneous surface chemistry of nanocarbon. The TEM images of (a) CNTs, (b) NCNTs, and (c) OCNTs; The XPS spectra of (d) survey scans comparing CNTs, NCNTs, and OCNTs located in N1s and O1s region, (e) the high-resolution N1s spectrum of NCNTs.

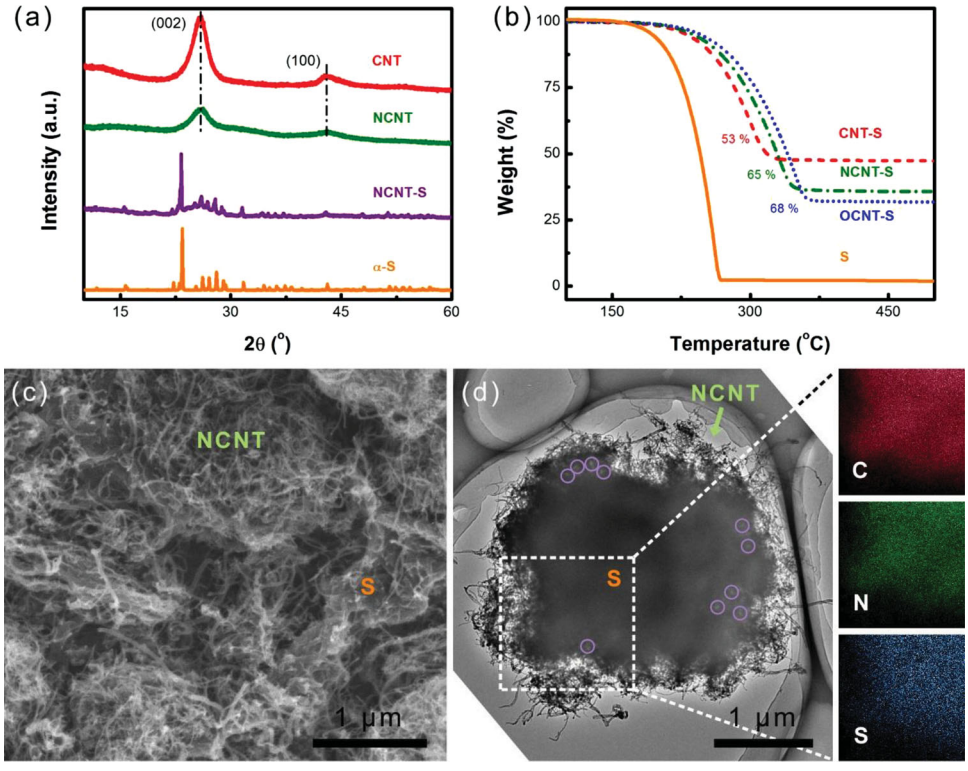

Figure 2. Heterogeneous carbon based composite sulfur cathode. (a) XRD patterns of CNTs, NCNTs, NCNT-S, and α-S; (b) TG curves of CNT-S, NCNT-S, OCNT-S, and S powders; (c) SEM, (d) TEM images, and corresponding EDS mapping of NCNT-S showing the morphology of composites and distribution status of S.

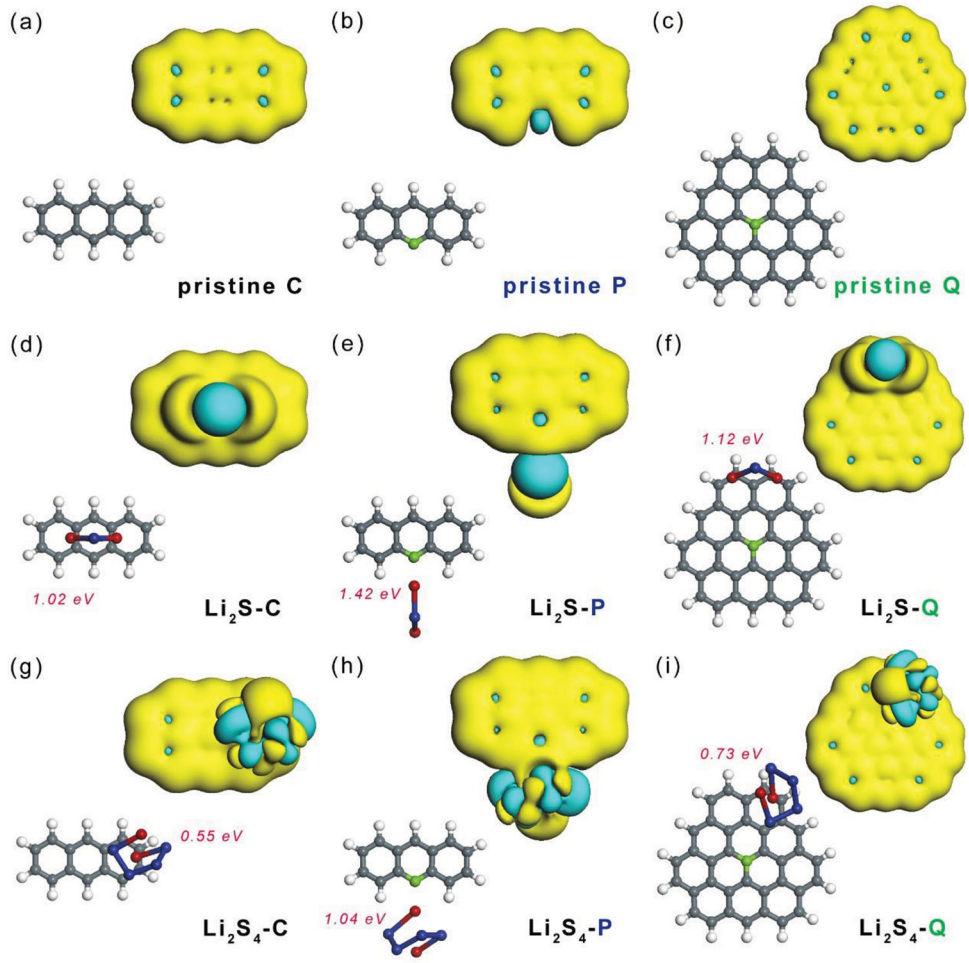

Figure 3. First-principle calculation of carbon host-sulfur containing guest interaction, showing the optimized molecular configuration and corresponding deformation charge density. Pristine molecular of (a) C, (b) P, and (c) Q, and corresponding pair with (d-f) Li_2S and (g-i) Li_2S_4. In molecular configuration, the numbers represent the binding energy between host and guest while the hydrogen, lithium, carbon, nitrogen, and sulfur atoms are denoted as spheres in white, red, dark grey, green, and blue respectively. In distribution of deformation charge density, donation/acceptance of electron is denoted as light yellow/cyan respectively.

thermogravimetric (TG) analysis indicated (Figure 2b). The strong affinity between S guests and electronically-meditated carbon host through N-/O-containing sites was proposed as the reason.[23,34] Hence, cathode material with high S content of over 65 wt% can be available while no extra conductive agent was added. SEM image of NCNT-S indicates that S is well distributed in NCNT scaffold with good electrical contact while no isolated bulk S particle is observed (Figure 2c). As shown in TEM image, elemental S and NCNT networks assemble into a micrometer-sized sphere, in which the interspace of NCNTs is partially occupied by uniformly dispersed S while remained mesoscale channels for ion transfer (denoted as violet circles) (Figure 2d). Corresponding to energy dispersive spectroscopic (EDS) mapping of selected region (denoted as white dashed box), dominated C and N instead of S are observed at the edge of NCNT-S microsphere due to the sublimation of S under high vacuum and electron beam irradiation of TEM, which further confirms the poor physical confinement of S by open-structured NCNT scaffold.

Since the doping atoms in nanocarbon has been demonstrated their capability on tuning the surface electron distribution of carbon material and subsequently changing the band gap, surface affinity, and catalytic properties,[23,30,31,35] their effects on tuning the interaction between carbon hosts and S-containing guests are proposed. Thus, the first principle calculations were performed based on density functional theory (DFT). As shown in **Figure 3**, three kinds of molecules are designed as simplified models to represent the undoped CNTs (C), pyridinic N region (P), and quaternary N region (Q) in NCNTs, respectively. S atom and Li_2S_x (x = 1–4) clusters with high polarity and positive charged terminal Li atoms (Figure S3) interacted with these three species to simulate the host-guest interaction. The binding energies of each adsorption pair are summarized in Table S3. For clarity, the optimized molecule configuration and deformation electron density of C, P, Q, and their binding pairs with Li_2S/Li_2S_4 are illustrated in Figure 3. Note that P and Q species are corroborated to possess higher binding energies (1.04~1.42 eV, 0.73~1.12 eV, respectively) with Li_2S_x than C species (0.55~1.02 eV), indicating that NCNTs with dominated pyridinic/quaternary N atoms exhibit much stronger affinity with polar Li_2S and polysulfide species

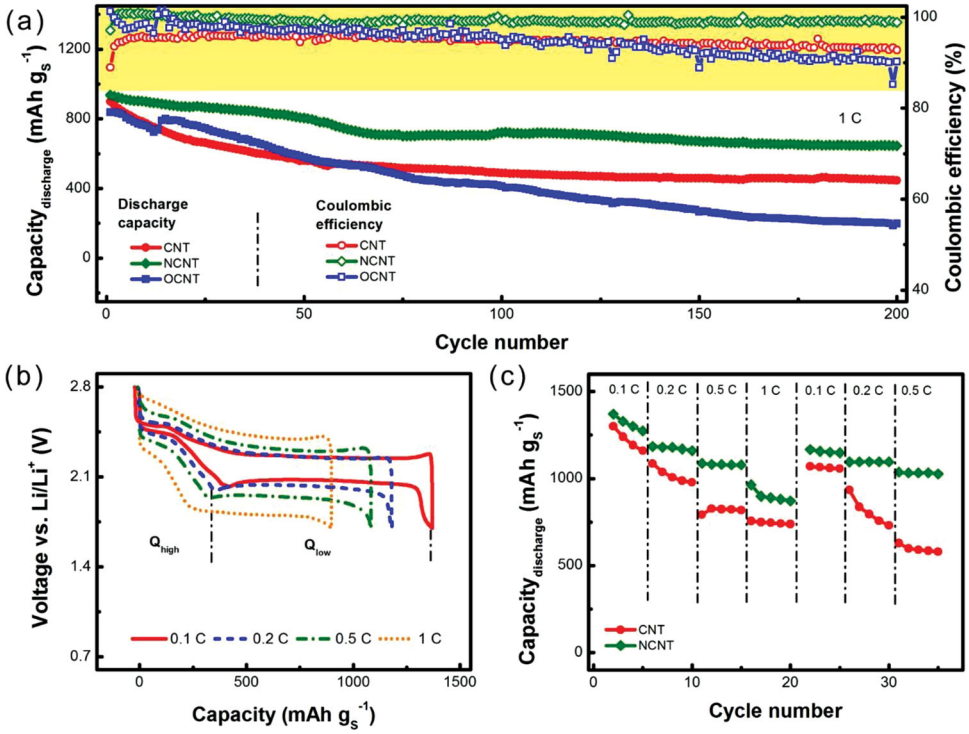

Figure 4. The electrochemical performance of CNT, NCNT and OCNT based composite cathodes. (a) The cycling performance at a current density of 1.0 C, (b) galvanostatic charge-discharge curves and (c) rate performance of CNT based cathode with different current densities.

than pristine CNTs (Table S3). For the pyridinic N, the most stable configuration of P and Li_2S_x turns out to be highly positive charged Li atom binding directly to the electron-rich pyridinic N with a lone pair electrons, suggesting a strong interaction derived from electron donating/accepting between Li in Li_2S_x and pyridinic N located in edges of graphene plane (Figure 3e, h). While for the quaternary N, S-containing polar species are more likely adsorbed on the neighboring carbon surface since the substituted quaternary N plays as an electron donor and provides an additional electron to the delocalized π-system, which modulates the electron distribution of the host-guest interface (Figure 3f, i). Although the Li_2S and polysulfides cannot be adsorbed by quaternary N directly, the electron distribution of neighboring delocalized π-system is affected by the substitution of central N atom, thus exhibits higher affinity to polar species than original graphene plane. The exchange of electron surrounding the adsorption sites in P and Q is further confirmed in Figure S4. Moreover, the enhanced interaction potential between functionalized carbon surface and Li_2S_x is independent on where the doping site locates, for the electron is highly delocalized in continuous graphene plane. To simulate functionalized carbon surface more realistically, no special and complex configuration like previously reported O-functional groups adjacent to pyrolinic/pyridinic N is required.[23] Thus, N-doping renders the nanocarbon hosts with heterogeneous surface amphiphilic for both nonpolar S and polar polysulfides/Li_2S guests by atomically mediating the surface electron distribution, of which strongly-coupled interfaces lead to superior electrochemical performance involving phase-evolutionary Li-S chemistry.

With rationally designing and modulating the surface chemistry of nanocarbon skeleton, the electrochemical behavior of S composite cathode is dramatically facilitated. The pristine CNT-S cathode delivers an initial discharge capacity of 899 mAh g^{-1} at a current density of 1.0 C, while the NCNT-S and OCNT-S cathodes with even higher content of S exhibit compatible capacity of 937 and 838 mAh g^{-1} (**Figure 4**a). However, the cycling stability is significantly different. The NCNT-S cathode exhibits the most favorable cyclability of nearly 70% of capacity retention (645 mAh g^{-1}) after 200 cycles, while the capacity of CNT-S and OCNT-S decay rapidly to 640 mAh g^{-1} during the first 30 and 40 cycles, respectively. The cyclic degradation rate of NCNT-S, CNT-S, and OCNT-S cathode is 0.16, 0.25, and 0.38% during 200 cycles. Furthermore, the coulombic efficiency of NCNT-S cathode maintains over 99.2% during long-term cycling, demonstrating the high reversibility and efficiency. This suggests that the enhanced interaction between Li_2S/polysulfides and N-doping graphene plane is effective to restrain the shuttle effect. In contrast, CNT-S and OCNT-S cathode possess lower and declined coulombic efficiency, revealing the severer shuttling effects. Due to the strongly-coupled interface between S and N-doped carbon, NCNT-S cathode also exhibit an excellent and highly reversible rate performance of 1370, 1185, 1087, and 964 mAh g^{-1} at current density of 0.1, 0.2, 0.5, and 1.0 C, respectively (Figure 4b). Furthermore, no significant decline of capacity was observed when the current density reverted to lower 0.1, 0.2 and 0.5 C while the CNT-S cathode still suffer severe deterioration (Figure 4c).

The favorable cycling performance of NCNT-S far beyond CNT and OCNT based composite cathode is elucidated by

artificially revealing and decoupling the multi-phase and multi-step transfer chemistry. All of the galvanostatic charge-discharge curves exhibit typical two-plateaus profiles in which plateaus of 2.0–2.4 V and 1.8–2.0 V corresponding to the reduction of S to high-order polysulfides (Li_2S_x, x = 4–8) and subsequent transformation of Li_2S_4 to Li_2S respectively. However, the charge-discharge profiles are in different fading tendencies as mediating the surface properties of carbon hosts (Figure S5). Meanwhile, the potential barrier at the initial charge stage of NCNT-S is lower than CNT-S and OCNT-S, suggesting that the N-doping sites render a uniform nucleation of Li_2S strongly coupled on carbon surface, thus lower the resistance of charge transfer. Such differences shed a light on the mechanism of capacity fading. Generally, the discharge capacity involving multi-electron-transfer chemistry is determined by (i) the active material and (ii) intermediates participating in electrochemical reactions, as well as (iii) the number of electron transfer. Simplifying the discharge process in a Li-S cell as following two-step reaction (1–2), the capacity contribution of high plateau and low plateau is identified as Q_{high} and Q_{low}, respectively.

$$S + 0.5Li^+ + 0.5e^- \rightarrow 0.25Li_2S_4\,(Q_{high}) \quad (1)$$

$$0.25Li_2S_4 + (x-0.5)Li^+ + (x-0.5)e^- \rightarrow Li_xS\,(Q_{low}) \quad (2)$$

On one hand, Q_{high} corresponding to the reduction of S into Li_2S_4 indicates the participation of active phase, which is determined by (i) the accessibility of electron/ion on C/S interfaces and (ii) reversibility of Li_2S charging back to S or videlicet, rechargeability of active materials. Since the reaction can only occur at the interface near carbon hosts due to the low electronic/ionic conductivity of active phase, the Li_2S close to the conductive substrate is firstly oxidized into soluble polysulfides during charge process. The outer Li_2S may detach from the carbon scaffold with no contribution to capacity for succeeding cycles if the interaction between carbon and Li_2S is weak, resulting in loss of active material, electrical contact, and capacity decay. On the other hand, Q_{low} corresponding to the liquid-to-solid transformation of Li_2S_4 to Li_2S is determined by (i) the participation of S, (ii) participation of intermediate Li_2S_4, and (iii) the depth of lithiation. Considering that the polysulfides are metastable, highly reactive, thus easily lost while the liquid-to-solid transformation of Li_2S_4 to Li_2S is kinetically inert and slow, it's challenging to reach the theoretical value of Q_{low}. The whole capacity of S cathode (Q_{whole}) can be decoupled as shown in Equations (3–6).

$$Q_{whole} = 1675 \times P_S \times P_{Li_2S_4} \times D \quad (3)$$

$$Q_{high} = 419 \times P_S \quad (4)$$

$$Q_{low} = 1256 \times P_S \times P_{Li_2S_4} \times D \quad (5)$$

$$Q_{low} / Q_{high} = 3 \times P_{Li_2S_4} \times D \quad (6)$$

The P_S and P_{Li2S4} represent the participation of S and Li_2S_4, respectively. The depth of discharge D is identified as 0.5, 1, and 0.5–1 when the final discharge product is Li_2S_2, Li_2S, and their mixture. Thus, the deterioration of capacity induced by the loss of active material and decreased depth of lithiation is decoupled and elaborated in **Figure 5**a and b, respectively. The

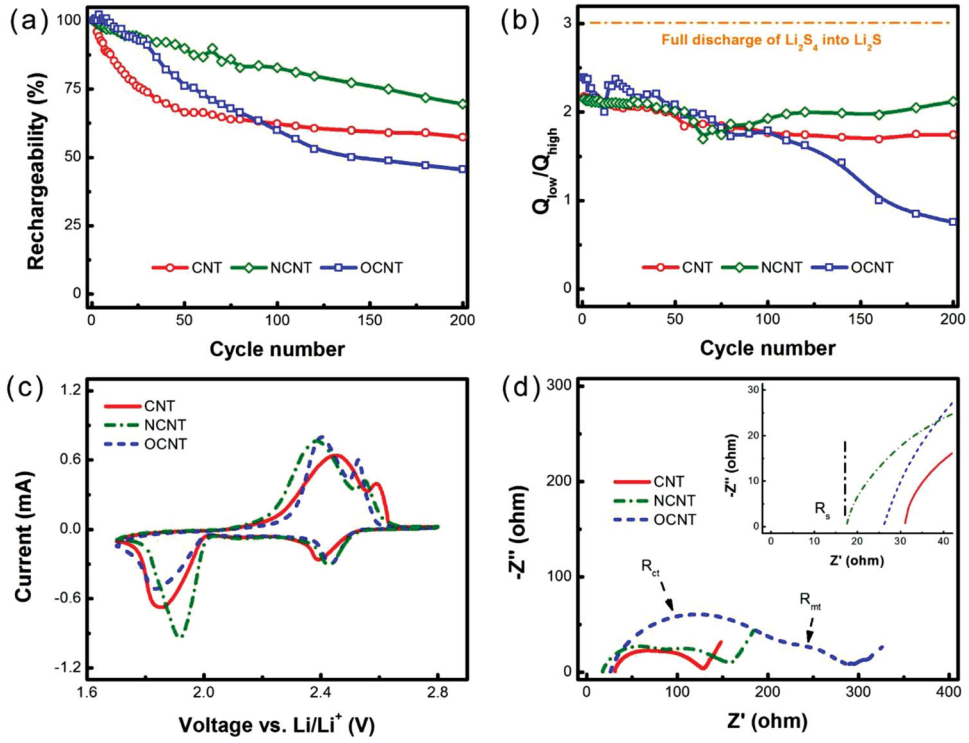

Figure 5. The different electrochemical behaviors of CNT, NCNT, and OCNT based composite cathodes. (a) Rechargeability of S/Li_2S during cycling at current density of 1.0 C. (b) Ratio of Q_{low} and Q_{high} of discharge curves of different cycles showing the participation of Li_2S_4 and depth of discharge. (c) CV profiles, (d) EIS spectra after 5 cycles.

rechargeability of S is normalized by dividing P_S of each cycles with the initial P_S at a current density of 1.0 C. As Figure 5a and S6 suggesting, NCNTs possess highest initial P_S over 70% and higher retention of S than raw CNTs and OCNTs, which is ascribed to the strong interaction between Li_2S and N-modified carbon surface. Li_2S strongly anchored on the N-doped CNTs can be reversibly charged back to S with good electrical contact for sustainable utilization, demonstrating the favorable rechargeability. Note that the retention of OCNTs becomes even worse than CNTs after 80 cycles, suggesting the poor conductivity of OCNTs deteriorates the re-nucleation of S although the S is strongly anchored to O-containing groups initially. Figure 5b illustrates the tendency of Q_{low}/Q_{high} during long-term cycling, which reveals the synergetic effect of leakage of polysulfide and limitation of lithiation. The NCNT-S exhibits high and stable Q_{low}/Q_{high} around 2.1, which is 20 and 180% higher than CNT and OCNT based cathode, respectively. This is attributed to the stronger adsorption of polar polysulfides on hetero N-modified carbon interface, rendering higher utilization of intermediate Li_2S_4 and full transformation on the interface. Meanwhile, NCNTs with moderate N-doping by CVD rather than nitric acid oxidation still maintain good conductivity of 798 S m^{-1} compared to pristine CNTs (1185 S m^{-1}). While the low conductivity of OCNTs (381 S m^{-1}) hinders the full lithiation of Li_2S_4 to Li_2S although O-containing groups have been proved the anchoring effects on polysulfides by applying graphene oxides or other similar oxygenated carbon based composites elsewhere.[10,36]

The cyclic voltammetric (CV) profiles are measured to interpret the electrochemical behavior (Figure S7). Two pairs of distinct redox peaks are observed and stabilize after the first cycle, in which the cathodic peaks around 2.40–2.43 V and the anodic peaks around 2.53–2.59 V are assigned to the transition between S and high-order polysulfides (Li_2S_x, x = 4–8) while the cathodic peaks around 1.83–1.92 V and the anodic peaks around 2.38–2.45 V correspond on the transformation between Li_2S_4 and solid Li_2S/Li_2S_2, respectively. The NCNT-S cathode exhibits relatively suppressed polarization, high redox intensities, and almost overlapped positions of redox peaks, demonstrating high reversibility, favorable electrode dynamics, and good stability (Figure S7b). In contrast, the CNT-S suffers unfavorable polarization and lower reversibility due to the lack of functional groups for enhanced interaction between S-containing guests and carbon hosts. While the low conductivity of OCNT renders unstable and inferior liquid-to-solid phase conversion process as the weak cathodic peaks at 1.83 V and high overpotential indicate (Figure 5c).

In addition, the electrochemical impedance spectra (EIS) also reveals such differences on electrochemical reaction and corresponding phase evolution, in which (i) the intercept and the semi-circles located in (ii) high-frequency and (iii) middle-frequency region are assigned to the impedance of cell components (R_s), charge transfer through the conductive scaffold and interfaces (R_{ct}), and mass transportation dominating the liquid-to-solid transformation through insoluble Li_2S_2/Li_2S (R_{mt}), respectively (Figure 5d).[13,37] The NCNT-S possesses much lower R_s than CNT-S and OCNT-S, indicating the less dissolution of high viscous polysulfides into the bulk phase of electrolytes which will increase R_s. While the R_{ct} of NCNT-S is significantly smaller than OCNT-S while only slightly higher than CNT-S, remaining stable and efficient charge transfer in continuous cycling. Consequently, a stable surface redox reaction is manipulated. The difference in R_{ct} is in good accordance with conductivity of CNTs, NCNTs, and OCNTs. Functionalized NCNT and OCNT based cathode show higher impedance of R_{mt} than CNT-S. This can be interpreted as that enriched polysulfides around functional groups retard ion diffusion due to the low ionic conductivity of polysulfides. Generally by using EIS, NCNT-S composite cathode demonstrates most favorable Li-S battery chemistry such as less leakage of polysulfides into electrolyte due to the immobilizing effect of doped N and moderate charge/mass transfer for stable surface reactions.

By engineering N-doped nanocarbon for Li-S cathode, strongly-coupled interface between modified carbon host and S-containing guest renders superior electrochemical performance especially the cycling stability. The role of C/S containing species interface is proposed as follows (**Figure 6**).

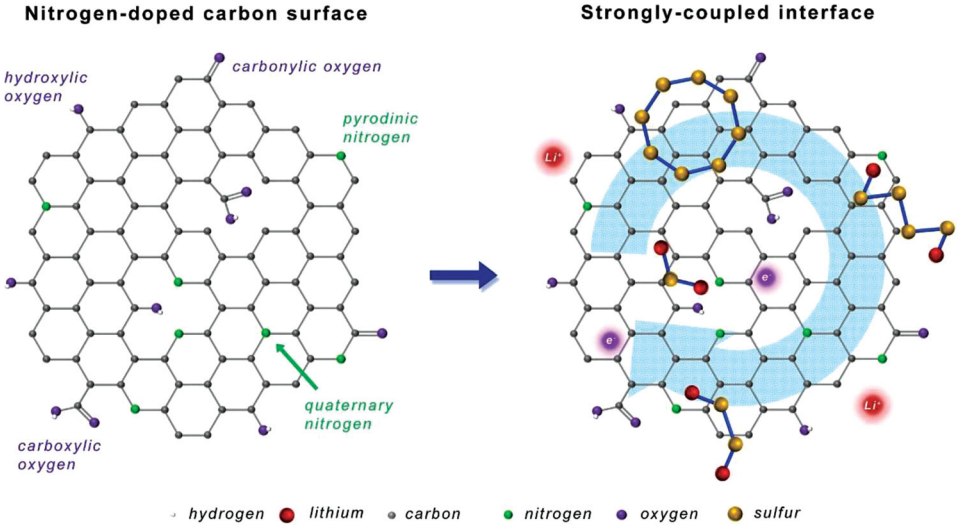

Figure 6. Schematic illustration of strongly coupled interfaces between N-doped carbon host and S-containing guest for highly stable Li-S battery.

Firstly, both the predominant pyridinic N and quaternary N in carbon lattice of NCNTs modify the electron distribution, enhance the affinity for insulative Li_2S as the first-principle calculation indicated, and eventually improve the reversibility of Li_2S recharging back to S. The strongly anchored Li_2S reduces the loss of active mass and maintain good electrical contact. Moreover, doping N atoms can also play a role of promoter for facile electron transfer as demonstrated in electrocatalytic applications (*e.g.* oxygen reduction reactions, fuel cells, etc),[31] which is indicated by reduced potential barrier at the initial stage of charge. Secondly, positive charged Li in polysulfides tends to be adsorbed by negatively charged pyridinic N and carbon surface around quaternary N. Hence, effective chemical gradient is built by these appropriate N-containing functional groups for trapping the polysulfides, resulting in higher retention of Q_{low} and high coulombic efficiency. Furthermore, the O-containing functional groups introduced spontaneously with N-doping can also immobilize S by the proposed weak chemical interaction as previously reported,[23,34] which is beneficial for good distribution of S during repeated phase evolution in discharge and charge. CNTs cannot serve as such multifunctional scaffold while the full demonstration of O-containing functional groups in OCNTs is hindered by the poor conductivity. In fact, the doping N in carbon skeleton not only simply provides extra electron to increase electron density with enhanced interaction to S-containing guests, but also, of the most importance, renders inhomogeneity of electron distribution towards heterogeneous conductive surface with amphiphilic affinity to all kinds of S species generated in the whole electrochemical and phase-change process. The difference in electronegativity of C and N induces disproportion of surface electrons, resulting in different functional regions for trapping S species with different polarities. Thus, the whole surface reaction and phase evolution at the active phase/conductive scaffold interface is well manipulated for stable Li-S cell performance. Compared to amphiphilic modification[24,26] by poly(vinylpyrrolidone) or polypyrrole polymer, which may lower the S content in composite cathode, *in-situ* modification of carbonaceous framework by N-doping provides similar chemical interaction with S-containing guests for stable cyclability while without sacrificing the energy density. Further investigation on N-doped nanocarbon with higher specific surface area, excellent conductivity, and more abundant pyridinic N functional groups are required to realize the rational combination of the benefiting effects such as abundant reactive interface and facile modified surface chemistry towards a Li-S cell with high capacity and stability. The mechanistic insight into the capacity fading will also inspire the rational design on electrode interface and N-doped carbon for other high-energy systems suffering from short lifespan, poor sustainability, and related issues on electron transfer and phase evolution such as Li-air battery and organic Li battery.

3. Conclusions

A novel strategy towards highly stable Li-S batteries was developed by building a strongly coupled interface between surface-mediated carbon hosts and various S-containing guests. Compared to CNTs and OCNTs, NCNTs with N-heterogenization were employed as a promising conductive host to accommodate sulfur guests with a high content of 65 wt% (58.5 wt% in the whole cathode), exhibiting a highly reversible, efficient, and stable Li storage properties such as mitigated polarization, high capacity of 1370 and 964 mAh g^{-1} at 0.1 and 1.0 C and 70% of capacity retention after 200 cycles. The outstanding reversibility and stability of NCNT-S cathode is attributed to the favorable guest-host interaction at the N-doped C/S interface, manifesting as (i) a chemical gradient to adsorb polar polysulfides and (ii) ameliorative deposition and recharging of Li_2S on the region of electron-rich pyridinic N and graphene surrounding quaternary N. First-principle calculations combined with electrochemical analysis were conducted to elucidate the host-guest interaction. Mechanistic insights into the capacity degradation induced by interface/phase evolution will give rise to further investigation on hierarchical composite electrodes based on the rational combination of conductive sp^2 nanocarbon/polymer host with loading guests to provide the optimized interfaces with high activity and good stability for Li-S cells, Li-air batteries, Li-ion batteries, supercapacitors, and solar cells.

Experimental Section

Synthesis of CNTs, NCNTs, and OCNTs: The synthesis of CNT/NCNT was carried out by a previously-reported catalytic CVD in fluidized bed with/without ammonia assistance using FeMgAl layered double hydroxide as catalysts and ethylene as carbon sources.[38] The OCNT was fabricated by chemical oxidation of raw CNTs by nitric acid of 7.5 mol L^{-1} for 30 min at 70 °C.

Fabrication of C/S Cathode Material: The C/S cathode materials were fabricated with a typical melt-diffusion strategy. The nanocarbon were firstly mixed with sulfur powder with a mass ratio of 3 : 7 by milling. The mixture was subsequently placed in a sealed flask at 155 °C for 4.0 h to incorporate S into the carbonaceous matrix.

Characterizations: The morphology of the samples was characterized by a JEM 2010 (JEOL Ltd, Tokyo, Japan) TEM operated at 120.0 kV. XRD patterns were recorded on a Bruker D8 Advance diffractometer at 40.0 kV and 120 mA with Cu-Kα radiation. The pore-size distribution and BET specific surface area of the samples were measured by N_2 adsorption/desorption using Autosorb-IQ2-MP-C system. The pore size distribution and pore volume of the nanocarbon samples were calculated by the quenched solid state functional theory (QSDFT) method. The TG analysis was carried out on the samples using TGA/DSC1 STARe system under N_2 atmosphere. The conductivity measurements of nanocarbon disk pre-compressed at 5 MPa were performed using the KDY-1 four-probe technique.

Calculations: The first principle calculations were conducted, using Perdew–Burke–Ernzerhof (PBE) exchange-correlation functional in the framework of general gradient approximation (GGA) implemented in the DMol3 package in Materials Studio (version 5.5) of Accelrys Inc.[39] An all-electron double numerical basis set with polarization functions (double numerical polarization (DNP) basis set) was used in this work. The convergence criteria applied for geometry optimizations were 1.0×10^{-5} au, 2.0×10^{-3} au $Å^{-1}$, and 5.0×10^{-3} Å for energy change, maximum force and maximum displacement, respectively. The threshold for self-consistent-field (SCF) density convergence was set to 1.0×10^{-6} eV and the global cutoff was set to fine. For quantitatively measuring the interaction between the CNT/NCNT and Li_2S_x (x = 1–4), we defined the binding energy E_b as follows:

$$E_b = E(C) + E(S) - E(\text{total}) \quad (7)$$

E(C), E(S), and E(total) represent the total energies of a polyaromatic molecule, an isolated Li_2S_x cluster or a S atom, and a polyaromatic molecule binding to a S-containing cluster, respectively.

Electrochemical Measurements: Two-electrode cells using standard 2025 coil-type cells were constructed to evaluate the electrochemical performance of the cathode materials for Li-S batteries. The cathode slurry was prepared by mixing 90% of the C/S materials and 10% of the poly(vinylidene fluoride) (PVDF) binder in a *N*-methyl-pyrrolidone (NMP) solvent dispersant. The positive electrodes were fabricated by coating the slurry on aluminum foil and drying at 60 °C for 12 h. A 1 mol L^{-1} lithium trifluoromethanesulfonate ($LiCF_3SO_3$) and 0.25 mol L^{-1} $LiNO_3$ solution in tetraethylene glycol dimethyl ether (TEGDME) was used for electrochemical evaluation. Lithium metal foil was used as the anode and the Celgard 2400 membranes from Celgard Inc. were used as the separators. The coin cells were tested in galvanostatic mode at various currents within a voltage range of 1.7–2.8 V using Neware multichannel battery cycler. The CV and EIS measurements were performed on Solartron 1470E electrochemical workstation at a scan rate of 0.1 mV s^{-1}. A current density of 1672 mA g^{-1} (1.0 C) equivalent to full discharge or charge in one hour was applied in both current sweep directions. The capacities were calculated based on the mass of S in the cathode.

Supporting Information

Supporting Information is available from the Wiley Online Library or from the author.

Acknowledgements

We thank helpful discussion with Prof. Feng Li, Dr. Guangmin Zhou, Xin-Yan Liu and Lin Zhu. This work was supported by the National Natural Science Foundation of China (21306103) and China Postdoctoral Science Foundation (2012M520293, 2013T60125).

Received: May 7, 2014
Revised: June 12, 2014
Published online: July 24, 2014

[1] P. G. Bruce, S. A. Freunberger, L. J. Hardwick, J. M. Tarascon, *Nat. Mater.* **2012**, *11*, 19.

[2] a) Y. Yang, G. Zheng, Y. Cui, *Chem. Soc. Rev.* **2013**, *42*, 3018; b) D. W. Wang, Q. C. Zeng, G. M. Zhou, L. C. Yin, F. Li, H. M. Cheng, I. Gentle, G. Q. Lu, *J. Mater. Chem. A* **2013**, *1*, 9382; c) S. Evers, L. F. Nazar, *Accounts. Chem. Res.* **2013**, *46*, 1135; d) A. Manthiram, Y. Z. Fu, Y. S. Su, *Acc. Chem. Res.* **2013**, *46*, 1125; e) M. K. Song, E. J. Cairns, Y. Zhang, *Nanoscale* **2013**, *5*, 2186.

[3] a) Y.-X. Yin, S. Xin, Y.-G. Guo, L.-J. Wan, *Angew. Chem. Int. Ed.* **2013**, *52*, 13186; b) S. S. Zhang, *J. Power Sources* **2013**, *231*, 153.

[4] Q. Zhang, J.-Q. Huang, W.-Z. Qian, Y.-Y. Zhang, F. Wei, *Small* **2013**, *9*, 1237.

[5] a) X. Ji, K. T. Lee, L. F. Nazar, *Nat. Mater.* **2009**, *8*, 500; b) J. T. Lee, Y. Zhao, S. Thieme, H. Kim, M. Oschatz, L. Borchardt, A. Magasinski, W.-I. Cho, S. Kaskel, G. Yushin, *Adv. Mater.* **2013**, *25*, 4573.

[6] a) W. Weng, V. G. Pol, K. Amine, *Adv. Mater.* **2013**, *25*, 1608; b) N. Jayaprakash, J. Shen, S. S. Moganty, A. Corona, L. A. Archer, *Angew. Chem. Int. Ed.* **2011**, *50*, 5904; c) K. Xi, S. Cao, X. Y. Peng, C. Ducati, R. V. Kumar, A. K. Cheetham, *Chem. Commun.* **2013**, *49*, 2192; d) C. Zhang, H. B. Wu, C. Yuan, Z. Guo, X. W. Lou, *Angew. Chem. Int. Ed.* **2012**, *51*, 9592; e) F. Bottger-Hiller, P. Kempe, G. Cox, A. Panchenko, N. Janssen, A. Petzold, T. Thurn-Albrecht, L. Borchardt, M. Rose, S. Kaskel, C. Georgi, H. Lang, S. Spange, *Angew. Chem. Int. Ed.* **2013**, *52*, 6088; f) J. Schuster, G. He, B. Mandlmeier, T. Yim, K. T. Lee, T. Bein, L. F. Nazar, *Angew. Chem. Int. Ed.* **2012**, *51*, 3591.

[7] a) J. Guo, Y. Xu, C. Wang, *Nano Lett.* **2011**, *11*, 4288; b) G. Zheng, Y. Yang, J. J. Cha, S. S. Hong, Y. Cui, *Nano Lett.* **2011**, *11*, 4462.

[8] a) G. M. Zhou, D. W. Wang, F. Li, P. X. Hou, L. C. Yin, C. Liu, I. Gentle, G. Q. Lu, H. M. Cheng, *Energy Environ. Sci.* **2012**, *5*, 8901; b) X. B. Cheng, J. Q. Huang, Q. Zhang, H. J. Peng, M. Q. Zhao, F. Wei, *Nano Energy* **2014**, *4*, 65; c) S. Dorfler, M. Hagen, H. Althues, J. Tubke, S. Kaskel, M. J. Hoffmann, *Chem. Commun.* **2012**, *48*, 4097; d) G. Y. Xu, B. Ding, P. Nie, L. F. Shen, J. Wang, X. G. Zhang, *Chem. Eur. J.* **2013**, *19*, 12306.

[9] a) H. Wang, Y. Yang, Y. Liang, J. T. Robinson, Y. Li, A. Jackson, Y. Cui, H. Dai, *Nano Lett.* **2011**, *11*, 2644; b) J. Q. Huang, X. F. Liu, Q. Zhang, C. M. Chen, M. Q. Zhao, S. M. Zhang, W. C. Zhu, W. Z. Qian, F. Wei, *Nano Energy* **2013**, *2*, 314; c) C. Zhang, W. Lv, W. Zhang, X. Zheng, M.-B. Wu, W. Wei, Y. Tao, Z. Li, Q.-H. Yang, *Adv. Energy Mater.* **2014**, *4*, 1301565; d) W. Lv, Z. Li, G. Zhou, J.-J. Shao, D. Kong, X. Zheng, B. Li, F. Li, F. Kang, Q.-H. Yang, *Adv. Funct. Mater.* **2014**, *22*, 3456.

[10] a) L. W. Ji, M. M. Rao, H. M. Zheng, L. Zhang, Y. C. Li, W. H. Duan, J. H. Guo, E. J. Cairns, Y. G. Zhang, *J. Am. Chem. Soc.* **2011**, *133*, 18522; b) G. Zhou, L.-C. Yin, D.-W. Wang, L. Li, S. Pei, I. R. Gentle, F. Li, H.-M. Cheng, *ACS Nano* **2013**, *7*, 5367.

[11] M. Q. Zhao, Q. Zhang, J. Q. Huang, G. L. Tian, J. Q. Nie, H. J. Peng, F. Wei, *Nat. Commun.* **2014**, *5*, 3410.

[12] a) J. L. Wang, J. Yang, J. Y. Xie, N. X. Xu, *Adv. Mater.* **2002**, *14*, 963; b) L. Xiao, Y. Cao, J. Xiao, B. Schwenzer, M. H. Engelhard, L. V. Saraf, Z. Nie, G. J. Exarhos, J. Liu, *Adv. Mater.* **2012**, *24*, 1176; c) W. Zhou, Y. Yu, H. Chen, F. J. DiSalvo, H. D. Abruna, *J. Am. Chem. Soc.* **2013**, *135*, 16736; d) W. D. Zhou, Y. C. Yu, H. Chen, F. J. DiSalvo, H. D. Abruna, *J. Am. Chem. Soc.* **2013**, *135*, 16736.

[13] W. Li, Q. Zhang, G. Zheng, Z. W. Seh, H. Yao, Y. Cui, *Nano Lett.* **2013**, *13*, 5534.

[14] a) M. Q. Zhao, X. F. Liu, Q. Zhang, G. L. Tian, J. Q. Huang, W. C. Zhu, F. Wei, *ACS Nano* **2012**, *6*, 10759; b) J.-Q. Huang, Q. Zhang, S.-M. Zhang, X.-F. Liu, W. Zhu, W.-Z. Qian, F. Wei, *Carbon* **2013**, *58*, 99; c) J. Q. Huang, H. J. Peng, X. Y. Liu, J. Q. Nie, X. B. Cheng, Q. Zhang, F. Wei, *J. Mater. Chem. A* **2014**, *2*, 10869; d) S. T. Lu, Y. W. Cheng, X. H. Wu, J. Liu, *Nano Lett.* **2013**, *13*, 2485; e) T. Xu, J. Song, M. L. Gordin, H. Sohn, Z. Yu, S. Chen, D. Wang, *ACS Appl. Mater. Interfaces* **2013**, *5*, 11355.

[15] H. J. Peng, J. Q. Huang, M. Q. Zhao, Q. Zhang, X. B. Cheng, W. Z. Qian, F. Wei, *Adv. Funct. Mater.* **2014**, *24*, 2772.

[16] S. Xin, L. Gu, N. H. Zhao, Y. X. Yin, L. J. Zhou, Y. G. Guo, L. J. Wan, *J. Am. Chem. Soc.* **2012**, *134*, 18510.

[17] Z. W. Seh, W. Li, J. J. Cha, G. Zheng, Y. Yang, M. T. McDowell, P.-C. Hsu, Y. Cui, *Nat. Commun.* **2013**, *4*, 1331.

[18] X. Ji, S. Evers, R. Black, L. F. Nazar, *Nat. Commun.* **2011**, *2*, 325.

[19] a) Y.-S. Su, A. Manthiram, *Nat. Commun.* **2012**, *3*, 1166; b) G. Zhou, S. Pei, L. Li, D.-W. Wang, S. Wang, K. Huang, L.-C. Yin, F. Li, H.-M. Cheng, *Adv. Mater.* **2014**, *26*, 625.

[20] Z. Lin, Z. Liu, N. J. Dudney, C. Liang, *ACS Nano* **2013**, *7*, 2829.

[21] L. M. Suo, Y. S. Hu, H. Li, M. Armand, L. Q. Chen, *Nat. Commun.* **2013**, *4*, 1481.

[22] D. Aurbach, E. Pollak, R. Elazari, G. Salitra, C. S. Kelley, J. Affinito, *J. Electrochem. Soc.* **2009**, *156*, A694.

[23] J. Song, T. Xu, M. L. Gordin, P. Zhu, D. Lv, Y. B. Jiang, Y. S. Chen, Y. Duan, D. Wang, *Adv. Funct. Mater.* **2014**, *24*, 1243.

[24] a) G. Zheng, Q. Zhang, J. J. Cha, Y. Yang, W. Li, Z. W. Seh, Y. Cui, *Nano Lett.* **2013**, *13*, 1265; b) Z. W. Seh, H. T. Wang, P. C. Hsu, Q. F. Zhang, W. Y. Li, G. Y. Zheng, H. B. Yao, Y. Cui, *Energy Environ. Sci.* **2014**, *7*, 672.

[25] G. Y. Zheng, Q. F. Zhang, J. J. Cha, Y. Yang, W. Y. Li, Z. W. Seh, Y. Cui, *Nano Lett.* **2013**, *13*, 1265.
[26] Z. W. Seh, Q. Zhang, W. Li, G. Zheng, H. Yao, Y. Cui, *Chem. Sci.* **2013**, *4*, 3673.
[27] J.-Q. Huang, Q. Zhang, H.-J. Peng, X.-Y. Liu, W.-Z. Qian, F. Wei, *Energy Environ. Sci.* **2014**, *7*, 347.
[28] a) X. G. Sun, X. Q. Wang, R. T. Mayes, S. Dai, *ChemSusChem* **2012**, *5*, 2079; b) F. G. Sun, J. T. Wang, H. C. Chen, W. C. Li, W. M. Qiao, D. H. Long, L. C. Ling, *ACS Appl. Mater. Interfaces* **2013**, *5*, 5630; c) N. Brun, K. Sakaushi, J. Eckert, M. M. Titirici, *ACS Sustainable Chem. Eng.* **2014**, *2*, 126; d) C. Tang, Q. Zhang, M. Q. Zhao, J. Q. Huang, X. B. Cheng, G. L. Tian, H. J. Peng, F. Wei, *Adv. Mater.* **2014**, doi: 10.1002/adma.201401243.
[29] P. Y. Zhu, J. X. Song, D. P. Lv, D. H. Wang, C. Jaye, D. A. Fischer, T. P. Wu, Y. S. Chen, *J. Phys. Chem. C* **2014**, *118*, 7765.
[30] D. S. Su, J. Zhang, B. Frank, A. Thomas, X. Wang, J. Paraknowitsch, R. Schloegl, *ChemSusChem* **2010**, *3*, 169.
[31] D. Yu, Q. Zhang, L. Dai, *J. Am. Chem. Soc.* **2010**, *132*, 15127.
[32] a) G. L. Tian, M. Q. Zhao, D. Yu, X. Y. Kong, J. Q. Huang, Q. Zhang, F. Wei, *Small* **2014**, *10*, 2251; b) L. Qie, W.-M. Chen, Z.-H. Wang, Q.-G. Shao, X. Li, L.-X. Yuan, X.-L. Hu, W.-X. Zhang, Y.-H. Huang, *Adv. Mater.* **2012**, *24*, 2047.
[33] C.-M. Chen, Q. Zhang, X.-C. Zhao, B. Zhang, Q.-Q. Kong, M.-G. Yang, Q.-H. Yang, M.-Z. Wang, Y.-G. Yang, R. Schloegl, D. S. Su, *J. Mater. Chem.* **2012**, *22*, 14076.
[34] C. Zu, A. Manthiram, *Adv. Energy Mater.* **2013**, *3*, 1008.
[35] X. Wang, X. Li, L. Zhang, Y. Yoon, P. K. Weber, H. Wang, J. Guo, H. Dai, *Science* **2009**, *324*, 768.
[36] R. Demir-Cakan, M. Morcrette, F. Nouar, C. Davoisne, T. Devic, D. Gonbeau, R. Dominko, C. Serre, G. Ferey, J. M. Tarascon, *J. Am. Chem. Soc.* **2011**, *133*, 16154.
[37] C. Barchasz, J. C. Lepretre, F. Alloin, S. Patoux, *J. Power Sources* **2012**, *199*, 322.
[38] G.-L. Tian, M.-Q. Zhao, Q. Zhang, J.-Q. Huang, F. Wei, *Carbon* **2012**, *50*, 5323.
[39] a) B. Delley, *J. Chem. Phys.* **1990**, *92*, 508; b) B. Delley, *J. Chem. Phys.* **2000**, *113*, 7756.